Measuring the dynamics of an XXZ quantum simulator and controlling collapse through symmetries

D. J. Papoular*
Laboratoire de Physique Théorique et Modélisation, UMR 8089 CNRS & CY Cergy Paris Université, 95302 Cergy–Pontoise, France
(Dated: August 5, 2025)

We theoretically consider the quantum simulation of a spin Hamiltonian whose twelve sites are arranged in a planar configuration with high spatial symmetry, D_{6h}. We map the system onto an effective fermionic Hamiltonian and identify its symmetry group. Comparing different initial states evolving under the Heisenberg or XXZ Hamiltonians, we analyze the impact of symmetry on the probability distribution for the outcomes of a measurement in a given basis, as a function of the evolution time. The considered measurement basis resolves only a part of the symmetries of the Hamiltonian. We show that, for suitable choices of the initial state, unresolved symmetries make some configurations equiprobable. We identify four different regimes for the time evolution of the probabilities: these may be constant, vary sinusoidally in time, evolve aperiodically, or collapse. We propose an experimentally accessible scheme which exploits quantum parallelism to probe these regimes efficiently.

The evolution in time of a quantum system in a given initial state crucially depends on their symmetries [1]. For example, the conservation of the total spin projection makes the ferromagnetic state an eigenstate of the Heisenberg Hamiltonian [2, chap. 33]. In the opposite limit, if the dynamics involves many eigenstates with different energies, the initial state collapses, as e.g. in the short–time dynamics of the Jaynes–Cummings Hamiltonian [3], observed in various atomic systems [4, 5].

Symmetry has been thoroughly investigated in atoms, molecules, and ordered condensed matter [1]. The eigenstates of a Hamiltonian H are classified in terms of their transformation properties under its symmetry group [6, chap. 11]. This explains the degeneracies of the energy spectrum of H. It also yields selection rules causing the various symmetry classes not to be coupled by the unitary quantum evolution. However, quantum measurements are subsequently performed in a specific basis [7, Sec. 2.2.3], dictated by experimental constraints, whose vectors may have projections along multiple symmetry classes. Then, the measurement cannot discriminate between these classes, and mixes them. Hence, the probabilities for the outcomes of a measurement, performed after quantum evolution of a given duration, do not directly reflect the symmetries of the system, but result from an interplay between these and the properties of the measurement basis. To our knowledge, the impact of high spatial symmetry on the time dependence of measurements performed in a basis resolving only part of the symmetries of the system has not yet been addressed.

This novel investigation has recently become accessible in ongoing experiments pertaining to the quantum simulation of spin Hamiltonians using magnetic atoms [8], Rydberg atoms [9, 10] or polar molecules [11, 12], and the recent proposal involving trapped circular Rydberg atoms [13], thanks to two essential properties. Firstly, they offer well–controlled systems with arbitrary spatial geometries [14] which may be devoid of translational invariance. Secondly, the quantum dynamics of these systems may be probed as a function of time by spatially–resolved imaging [11, 14] or non–destructive read–out [15]. In this context, we consider the quantum evolution of N trapped qubits followed by the measurement of their spin projections, which gives access to the projection of the total spin but neither to its modulus nor to spatial symmetries.

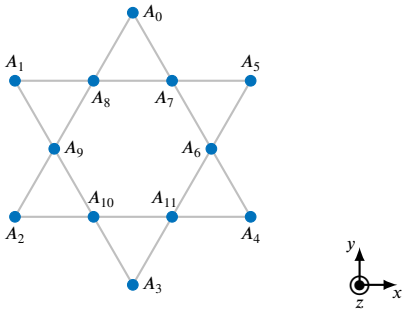

FIG. 1. Considered double–ring system: 12 interacting qubits (blue disks) trapped in the (x, y) plane in a geometry with D_{6h} symmetry. Each site A_i, located at the position $\boldsymbol{r}_i$, contains a single particle.

In this Letter, we theoretically identify the impact of unresolved symmetries on the measurement probabilities, as well as signals insensitive to them. We focus on the quantum simulation of a 12–qubit Heisenberg (H) or XXZ spin Hamiltonian [16, Sec. 1.4.1] trapped in the geometry of Fig. 1 exhibiting high spatial symmetry. We map the system onto an effective fermionic Hamiltonian. Then, for a given initial state, we analyze the probability distribution for the result of a quantum measurement in an experimentally accessible basis as a function of the duration of the quantum evolution. We show that symmetries unresolved by the measurement basis make some outcomes equiprobable. Considering different initial states and Hamiltonians, all experimentally accessible, we identify four different regimes for the measurement probabilities: these may be constant, vary sinusoidally in time, evolve aperiodically, or undergo a collapse. We propose a scheme exploiting quantum parallelism, relying on the resolved symmetries, to probe these regimes efficiently through repeated realizations starting from the same initial state.

Figure 1 does not exhibit translational invariance. It is a finite–sized fraction of the Kagome lattice currently investigated in the different context of frustration [17]. The number $N = 12$ of qubits it involves is well within experimental

range. Its essential feature is its double–ring structure: the sites A_0, …, A_5 and A_6, …, A_{11} respectively comprise the outer and inner rings. We show in the Supplemental Material (SM) [18, Sec. III] that it accommodates non–trivial quantum states which *(i)* are factorized in terms of individual qubit states and, hence, experimentally accessible [7, Sec. 1.5.2], and *(ii)* transform under a specific irreducible representation of the spatial symmetry group.

Considered system — We consider $N = 12$ bosonic or fermionic identical particles, confined in the (xy) plane at the nodes $(\boldsymbol{r}_i)_{0\leq i\leq N-1}$ of the regular six–branched star of Fig. 1. We neglect the spatial motion of the particles within the traps. Each particle i represents a qubit with two accessible quantum states $|\uparrow_i^z\rangle$ and $|\downarrow_i^z\rangle$. The particles exhibit pairwise interaction, whose strength depends on $r_{ij} = |\boldsymbol{r}_j - \boldsymbol{r}_i|$ through the power law $1/r_{ij}^\alpha$ with $\alpha > 0$. The N–particle Hamiltonian reads:

$$H = \frac{1}{2}\sum_{i\neq j}\left(\frac{a}{r_{ij}}\right)^\alpha \left[J(\sigma_i^x\sigma_j^x + \sigma_i^y\sigma_j^y) + J_z\,\sigma_i^z\sigma_j^z\right] , \qquad (1)$$

where $a = r_{08}$ is the nearest–neighbor distance. The Pauli operators $\boldsymbol{\sigma}_i = (\sigma_i^x, \sigma_i^y, \sigma_i^z)$ represent the qubit at $\boldsymbol{r}_i$, and J, J_z are constant energies. The Hamiltonian $H = H_{\rm H}$ or $H_{\rm XXZ}$ depending on whether $J = J_z$ or $J \neq J_z$. For our numerical calculations (Figs. 2 and 3), we take $\alpha = 6$, $J > 0$, and $-3 < J_z/J < 3$ as in Ref. [13], but these choices are not essential.

Effective fermionic model — We assume that the spatial wavefunctions of any two sites $i \neq j$ have negligible overlap. Then, the bosonic or fermionic nature of the particles plays no role [19, Sec. XIV.8]. The Hamiltonian H may be expressed in the basis $\mathfrak{c} = (|c_f\rangle)_{0\leq f\leq 2^N-1}$ comprising the 2^N configurations $|\boldsymbol{r}_0, \mu_0; \ldots; \boldsymbol{r}_{N-1}, \mu_{N-1}\rangle = |(\boldsymbol{r}_i, \mu_i)_{0\leq i\leq N-1}\rangle$ of N particles, particle i being at the site $\boldsymbol{r}_i$ in the state $|\mu_i\rangle = |\uparrow_i^z\rangle$ or $|\downarrow_i^z\rangle$, and the $\boldsymbol{r}_i$'s being ordered with increasing i. We have obtained all our numerical results using $\mathfrak{c}$. However, a spatial symmetry operation leaving the system globally invariant exchanges the positions of the N sites, mapping $(\boldsymbol{r}_i)_{0\leq i\leq N-1}$ onto $(\boldsymbol{r}_{\phi(i)})_{0\leq i\leq N-1}$ for some permutation ϕ of N elements. If $\phi \neq 1$, $|(\boldsymbol{r}_{\phi(i)}, \mu_i)_{0\leq i\leq N-1}\rangle \notin \mathfrak{c}$: we define it as $(-)^\phi\,|(\boldsymbol{r}_i, \mu_{\phi^{-1}(i)})_{0\leq i\leq N-1}\rangle$, with $(-)^\phi$ being the parity of ϕ. This maps H onto an effective lattice model for fermionic particles, described by the spin–1/2 operators $\boldsymbol{s}_i = \hbar\boldsymbol{\sigma}_i/2$ transforming through the usual rules [19, Secs. XIII.19 & XV.10].

Symmetry group — The unitary symmetries of H make up a spin–point group [20, 21] $G = G^{\rm spatial} \times G^{\rm spin}$, which is the direct product of the group $G^{\rm spatial}$ acting on the positions while leaving the spins invariant, and the group $G^{\rm spin}$ acting on the spins while leaving the positions invariant. Due to the lack of translational invariance, $G^{\rm spatial}$ is the point group D_{6h} [22, §93]. The continuous group [22, §98] $G^{\rm spin}$ is $D_{\infty h}$ if $J_z/J \neq 1$, and K_h, the group of complete spherical symmetry, if $J_z/J = 1$. For both D_{6h} and $D_{\infty h}$, the high–symmetry axis $\boldsymbol{e}_z$ is perpendicular to the plane of Fig. 1. To summarize:

$$G_{\rm H} = D_{6h}^{\rm spatial} \times K_h^{\rm spin} \text{ and } G_{\rm XXZ} = D_{6h}^{\rm spatial} \times D_{\infty h}^{\rm spin} . \qquad (2)$$

M	6	5	4	3	2	1	0
$d^{(\pm M)}$	1	12	66	220	495	792	924
$\delta_0[\chi^{(M)}]$	1	2	9	24	50	76	90
$\delta_0[\xi^{(\pm M)}]$	1	2	9	24	50	76	48

TABLE I. Dimensions of the subspaces $\mathcal{E}^{(M)}$, $\mathcal{H}_0[\chi^{(M)}]$, and $\mathcal{H}_0[\xi^{(M)}]$ for each total spin projection M. For $M < 0$, $\delta_0[\chi^M] = 0$.

The Hamiltonian H only has matrix elements between states transforming under the same irreducible representation ρ of $D_{6h}^{\rm spatial}$. The group $G^{\rm spin}$ yields conservation laws concerning the total spin operator $\boldsymbol{S} = \sum_{i=0}^{N-1}\boldsymbol{s}_i$. If $J_z \neq J$, only S_z is conserved, yielding the symmetry classes $s = (\rho, M)$, where the integer M satisfies $-N/2 \leq M \leq N/2$ and sets the total spin projection $S_z = \hbar M$. If $J_z = J$, $\boldsymbol{S}^2$ is also conserved, hence, each symmetry class is defined by $s = (\rho, S, M)$, where the integer S satisfies $0 \leq S \leq N/2$ and sets the total spin modulus $\boldsymbol{S}^2 = \hbar^2 S(S+1)$. In the SM [18, Sec. II], we analytically predict, in both cases, the dimensions of the symmetry classes and the degeneracies of the energy spectrum.

The system comprises an even number N of spins 1/2, hence, only single–valued representations intervene [22, §99]. The group $G^{\rm spin}$ contains the two–fold rotation $C_2^{\boldsymbol{e}_x,{\rm spin}}$ about $\boldsymbol{e}_x$, which simultaneously flips all N spin projections, causing any eigenstate of H with the total spin projection $M \neq 0$ to be twice degenerate at least (see SM [18, Sec. II]). The time–reversal operator, which is not in G, yields no additional degeneracy for systems with D_{6h} symmetry [23, Sec. 7.5].

Time dependence — We analyze the following protocol ($\mathcal{P}$). The system is initially in the N–particle state $|\psi_0\rangle$. It evolves under H. At time t, we measure its state $|\psi(t)\rangle$ in the basis $\mathfrak{c}$. The probability of finding $|c_f\rangle$ is $p_f(t) = |\,\langle c_f|\psi(t)\rangle\,|^2$, where

$$\langle c_f|\psi(t)\rangle = \sum_\nu \exp(-iE_\nu t/\hbar)\;\langle c_f|\Psi_\nu\rangle\,\langle\Psi_\nu|\psi_0\rangle\ . \qquad (3)$$

In Eq. (3), the $(|\Psi_\nu\rangle)_{0\leq\nu\leq N-1}$ are the eigenstates of H, with energies (E_ν). We choose each $|\Psi_\nu\rangle$ in a symmetry class s [22, §96]. However, most $|c_f\rangle$'s have components along multiple ρ and S, and so may $|\psi_0\rangle$. Thus, all s along which both $|\psi_0\rangle$ and $|c_f\rangle$ have non–zero projections contribute to the $(p_f(t))$'s. Nevertheless, symmetry has three important consequences: *(i)* it makes some configurations equiprobable, *(ii)* it allows for the probing of all $\mathcal{E}_M$'s in parallel, and *(iii)* for suitably chosen $|\psi_0\rangle$, it reduces the number of different frequencies entering Eq. (3). We now discuss these three consequences in turn.

Equiprobable outcomes — Let $\mathcal{H}_0[\psi_0]$ be the subspace spanned by all $|\Psi_\nu\rangle$'s such that $\langle\Psi_\nu|\psi_0\rangle \neq 0$, and P_0 the projector on $\mathcal{H}_0$. The $|c_f\rangle$'s and the $|\Psi_\nu\rangle$'s are real, hence, so is P_0. According to Eq. (3), if $P_0\,|c_{f_1}\rangle = \pm P_0\,|c_{f_2}\rangle$, then $p_{f_1}(t) = p_{f_2}(t)$ for all t. Therefore, only a subset of $\mathcal{N}_p[\psi_0]$ measurement outcomes $(|c_f\rangle)$ have different probabilities, with $\mathcal{N}_p[\psi_0] \geq \delta_0[\psi_0]$ and $\delta_0[\psi_0] = \dim\mathcal{H}_0$.

Parallel quantum simulation — The states $(|c_f\rangle)$ each have a well–defined $M_f = \sum_{i=0}^{N-1}\mu_i$, with $\mu_i = \pm 1/2$, hence,

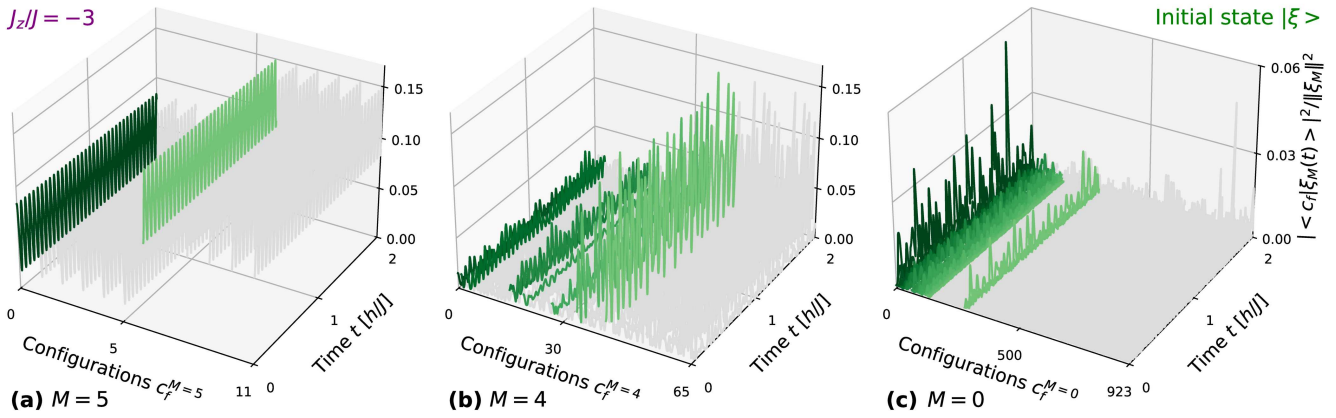

FIG. 2. Probabilities $p_f^{(M)}(t)$ of the $d^{(M)}$ outcomes $|c_f\rangle$ in $\mathcal{E}^{(M)}$, for the initial state $|\psi_0\rangle = |\xi\rangle$ evolving under $H_{\rm XXZ}$ with $\alpha = 6$ and $J_z/J = -3$, for $M =$ (a) 5, (b) 4, and (c) 0 (gray curves), rescaled such that $\sum_{f\in\mathcal{E}^{(M)}} p_f^{(M)}(t) = 1$. Single representatives of the $\delta_0[\xi^{(M)}]$ different functions $p_f^{(M)}(t)$ appear in shades of green. The probabilities for all other outcomes, each equiprobable to one of these, are shown in gray. Panels (a) and (b) illustrate sinusoidal and aperiodic behaviors, panel (c) shows that all rescaled $p_f^{(0)}(t) \leq 0.06$.

the subspaces $\mathcal{E}^{(M)}$ characterized by the total spin projections M are resolved by measurements in $\mathfrak{c}$. This allows for quantum parallelism [7, Sec. 1.4.2] as follows. We choose $|\psi_0\rangle = \sum_{M=-N/2}^{N/2} |\psi_0^{(M)}\rangle$ which is a superposition of up to $(N+1)$ components $|\psi_0^{(M)}\rangle \in \mathcal{E}^{(M)}$, coupled neither by the evolution nor by the measurement. We repeat protocol $(\mathcal{P})$ many times starting from the same initial state $|\psi_0\rangle$. We sort the measurement probabilities into $(N+1)$ families $(p_f^{(M)})$ related to the same $\mathcal{E}^{(M)}$, each comprising $d^{(M)} = \binom{N}{N/2+M}$ outcomes. The rescaled probabilities $[(p_f^{(M)}/(\sum_{f'} p_{f'}^{(M)})]$ of each family are equal to those obtained for the initial state $|\psi_0^{(M)}\rangle$.

Maximum number of frequencies entering the $p_f^{(M)}(t)$'s — To select a single ρ in Eq. (3), we choose $|\psi_0\rangle$ transforming under it. The projector $\boldsymbol{P}^{(M)}$ on $\mathcal{E}^{(M)}$ is a polynomial function of S_z [24, chap. VII], which commutes with the projector onto ρ [22, §94]. Thus, each $|\psi_0^{(M)}\rangle$ transforms under ρ. Then, all $|\Psi_\nu\rangle$ entering Eq. (3) for $|\psi^{(M)}(t)\rangle$ belong to the class (ρ, M), so that $\delta_0[\xi^{(M)}] \leq d_\rho^{(M)}$, with $d_\rho^{(M)} = \dim(\rho, M)$. Hence, the number $\mathcal{N}_\nu[\psi_0^{(M)}] = \delta_0[\psi_0^{(M)}](\delta_0[\psi_0^{(M)}] - 1)/2$ of different frequencies entering the $p_f^{(M)}(t)$'s is at most $d_\rho^{(M)}(d_\rho^{(M)} - 1)/2$.

Initial states — The ones most readily accessed in current experiments are products of single–particle states. In the SM [18, Sec. III], we identify a family of such states transforming under A_{2g}. We focus on two of these: $|\xi\rangle = |(\boldsymbol{r}_i, \uparrow_i^x)_{0\leq i\leq N-1}\rangle$ and $|\chi\rangle = |(\boldsymbol{r}_j, \uparrow_j^x)_{0\leq j\leq N/2-1}; (\boldsymbol{r}_k, \uparrow_k^z)_{N/2\leq k\leq N-1}\rangle$, where $|\uparrow_i^x\rangle = (|\uparrow_i^z\rangle + |\downarrow_i^z\rangle)/2^{1/2}$ is the eigenstate of s_i^x with the eigenvalue $+\hbar/2$. They may be prepared from the fully polarized state $|(\uparrow_i^z)_{0\leq i\leq N-1}\rangle$ by applying electromagnetic $\pi/2$–pulses to the individual qubits to be prepared in $|\uparrow^x\rangle$ [7, Sec. 1.5.2]. We now illustrate the preceding considerations on $|\xi\rangle$ and $|\chi\rangle$.

Different regimes for the time dependence of the p_f's. We first describe a situation with maximal symmetry: the initial state $|\xi\rangle$ evolving under $H_{\rm H}$, for which all p_f's are constant. Then, we consider two less symmetrical situations: either we replace $H_{\rm H}$ by $H_{\rm XXZ}$, or we replace $|\xi\rangle$ by $|\chi\rangle$. Four different regimes for the time dependence of the $p_f^{(M)}$'s are encountered, depending on the considered $|\psi_0\rangle$ and $\mathcal{E}_M$: constant probabilities, sinusoidal oscillation, aperiodicity, and collapse.

Symmetry achieves its maximal impact e.g. for the initial state $|\xi\rangle$ evolving under $H_{\rm H}$. The state $|\xi\rangle = \sum_{f=0}^{2^N-1} |c_f\rangle/2^{N/2}$, hence, $|\xi^{(M)}\rangle \neq 0$ for all $-N/2 \leq M \leq N/2$. It is the ferromagnetic state with all spins pointing along $|\uparrow^x\rangle$, which is an eigenstate of S_x, $\boldsymbol{S}^2$ and $H_{\rm H}$. Hence, the $p_f^{(M)}$'s are constant and equal, $p_f = |\langle c_f|\xi\rangle|^2 = 1/2^N$.

The impact of symmetry may be weakened in two different ways. Firstly, we keep the same initial state $|\psi_0\rangle = |\xi\rangle$, but turn to the Hamiltonian $H_{\rm XXZ}$. The state $|\xi\rangle$ is invariant under $C_2^{e_x,\rm spin}$, hence, $p_f^{(M)}(t) = p_f^{(-M)}(t)$. We find $\mathcal{N}_p[\xi^{(M)}] = \delta_0[\xi^{(M)}]$ for each M. Hence, the behavior of the $p_f^{(M)}(t)$'s depends on $\delta_0[\xi^{(M)}]$ (see Table I), which determines $\mathcal{N}_\nu[\xi^{(M)}]$ and $\mathcal{N}_p[\xi^{(M)}]$. The integer $\delta_0[\xi^{(6)}] = 1$, so that the single $p_f^{(\pm 6)}$ is constant. Figure 2, calculated for $J_z/J = -3$, illustrates the $p_f^{(M)}(t)$'s for $M = 5$, 4, and 0. In stark contrast to the case of the preceding paragraph, they are not constant. The integer $\delta_0[\xi^{(5)}] = 2$: two energies E_1, E_2 enter Eq. (3), yielding a sinusoidal oscillation at the same frequency $(E_1 - E_2)/h$ for all $d^{(5)} = 12$ $p_f^{(5)}(t)$'s, among which $\mathcal{N}_p[\xi^{(5)}] = 2$ are different. This sinusoidal regime reflects the Rabi oscillation between the two eigenstates in the class $(A_{2g}, M = 5)$, and the multipe outcomes in Fig. 2a signal that the measurement is not performed in a basis of states transforming under A_{2g}. We fully describe this regime analytically in the SM [18, Sec. V].

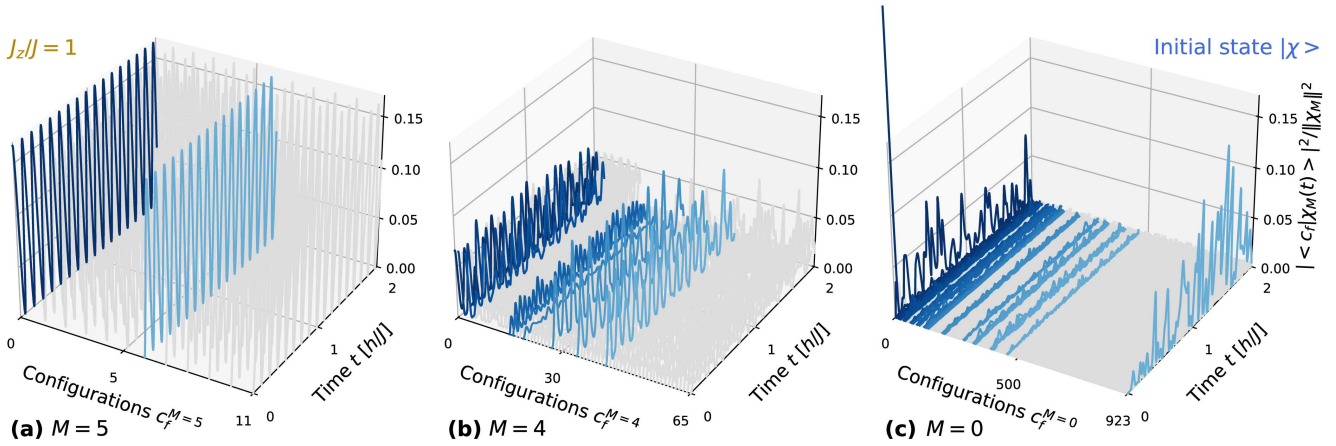

FIG. 3. Probabilities $p_f^{(M)}(t)$ of the $d^{(M)}$ outcomes $|c_f\rangle$ in $\mathcal{E}_M$, for the initial state $|\psi_0\rangle = |\chi\rangle$ evolving under $H_{\rm H}$ with $\alpha = 6$, for $M =$ (a) 5, (b) 4, and (c) 0 (gray lines), rescaled such that $\sum_{f\in\mathcal{E}^{(M)}} p_f^{(M)}(t) = 1$. Single representatives of the $\delta_0[\chi^{(M)}]$ different functions $p_f^{(M)}(t)$ appear in shades of blue. The probabilities for all other outcomes, each equiprobable to one of these, are shown in gray. Panels (a) and (b) illustrate sinusoidal and aperiodic behaviors, panel (c) shows a collapse of the initial quantum state $|\chi^{(0)}\rangle$.

For $M = 4$, the $d^{(4)} = 66$ aperiodic $p_f^{(4)}(t)$'s, among which $\mathcal{N}_p[\xi^{(4)}] = 9$ are different, involve $\mathcal{N}_\nu[\xi^{(4)}] = 36$ frequencies. For $M = 0$, the $p_f^{(0)}$'s involve $\mathcal{N}_\nu[\xi^{(0)}] = 1128$ frequencies $(E_\nu - E_{\nu'})/h$. The E_ν's, which all relate to the symmetry class $(M = 0, A_{2g})$, are independent. Accordingly, all probabilities $p_f^{(0)}(t) < 0.06$ at all times (see Fig. 2c), and no revival occurs, unlike for the Jaynes–Cummings Hamiltonian [25]. Concerning the short–term dynamics, all initial probabilities are equal, $p_f(t = 0) = 1/2^N$ as in the preceding paragraph, preventing the observation of a collapse of $|\xi^{(0)}\rangle$. We shall now overcome this difficulty by considering a different initial state.

Secondly, we turn to the initial state $|\chi\rangle$. It is the product of single–particle states which are the same on the six sites of each ring of Fig. 1, but different on the outer and inner rings, thus fully exploiting the double–ring structure. Its components $|\chi^{(M)}\rangle \neq 0$ for $0 \leq M \leq N/2$. We let $|\chi\rangle$ evolve under $H_{\rm H}$. The state $|\chi\rangle$ is not an eigenstate of $\boldsymbol{S}^2$, and accordingly, the $p_f^{(M)}$'s exhibit no clear signature of the fact that $H_{\rm H}$ conserves $\boldsymbol{S}^2$. In particular, for each $M \geq 0$, $\delta_0[\chi^{(M)}]$ exceeds $\delta_0[\xi^{(M)}]$ (see Table I) and actually achieves its maximum allowed value $d_{A_2}^{(M)}$. We again find $\mathcal{N}_p[\chi^{(M)}] = \delta_0[\chi^{(M)}]$. As previously, $p_f^{(6)}$ is constant. Figure 2 illustrates the time–dependent $p_f^{(M)}(t)$'s for $M = 5, 4$, and 0. The sinusoidal oscillation of Fig. 3a involves two eigenstates of $H_{\rm H}$ having $S = 6$ and 5, respectively (see SM [18, Table S4]), despite the conservation of S during the unitary evolution. The specificity of $|\chi\rangle$ appears for $M = 0$ (Fig. 3c), involving $\mathcal{N}_\nu[\chi^{(0)}] = 4005$ frequencies. Unlike $|\xi^{(0)}\rangle$, $|\chi^{(0)}\rangle$ reduces to the single configuration $|c_0^{(0)}\rangle = |(\boldsymbol{r}_j, \downarrow_j^z)_{0\leq j\leq N/2-1}; (\boldsymbol{r}_k, \uparrow_k^z)_{N/2\leq k\leq N-1}\rangle$, whose initial rescaled probability is 1. However, $|\chi^{(0)}\rangle$ quickly collapses, and $p_0^{(0)}(t)$ drops to very small values over a time $\sim 0.05h/J$. Subsequently, two configurations dominate: $|c_0^{(0)}\rangle$ and its spin–flipped configuration $|c_{923}^{(0)}\rangle$. Their probabilities evolve aperiodically, reaching values $\lesssim 0.15$. All other $p_f^{(0)}(t) \leq 0.035$. The dominance of $|c_0^{(0)}\rangle$ and $|c_{923}^{(0)}\rangle$ is itself a signature of symmetry, as they are the only two $M = 0$ configurations in $\mathfrak{c}$ exactly transforming under A_{2g}. As above, we expect no revival of the initial state $|\chi^{(0)}\rangle$ for long times. Values of $J_z/J \neq 1$ are expected to yield qualitatively similar behaviors for the $p_f^{(M)}(t)$'s (see SM [18, Fig. S2]).

Outlook — The two following points warrant further investigation. *(i)* The spatial motion of the trapped particles will also exhibit D_{6h} symmetry, allowing for the investigation of the impact of point–group symmetry on the coupling between spin and spatial dynamics [26]. *(ii)* In the Ising limit ($J = 0$), within the nearest–neighbor approximation ($\alpha \to \infty$), H has highly–degenerate eigenvalues. For $J_z > 0$, its ground state is 730–fold degenerate, signalling a strongly increased symmetry in this limit, which approximately survives for $\alpha = 6$.

We acknowledge stimulating discussions with M. Brune and J.M. Raimond (LKB, Collège de France), and with R.J. Papoular (IRAMIS, CEA Saclay).

* Electronic address: david.papoular@cyu.fr

[1] M. Tinkham, *Group theory and quantum mechanics* (McGraw-Hill (New York), 1964).
[2] N. W. Ashcroft and N. D. Mermin, *Solid State Physics* (Saunders (New York), 1976).
[3] F. W. Cummings, Stimulated emission of radiation in a single mode, Phys. Rev. **140**, A1051 (1965).
[4] M. Brune, F. Schmidt-Kaler, A. Maali, J. Dreyer, E. Hagley, J. M. Raimond, and S. Haroche, Quantum Rabi oscillation: a direct test of field quantization in a cavity, Phys. Rev. Lett. **76**, 1800 (1996).

[5] M. Greiner, O. Mandel, T. W. Hänsch, and I. Bloch, Collapse and revival of the matter wave field of a Bose-Einstein condensate, Nature **419**, 51 (2002).

[6] E. P. Wigner, *Group theory and its application to the quantum mechanics of atomic spectra* (Academic Press (New York), 1959).

[7] M. A. Nielsen and I. L. Chuang, *Quantum Computation and Quantum Information* (Cambridge University Press, Cambridge (UK), 2000).

[8] A. de Paz, A. Sharma, A. Chotia, E. Maréchal, J. H. Huckans, P. Pedri, L. Santos, O. Gorceix, L. Vernac, and B. Laburthe-Tolra, Nonequilibrium quantum magnetism in a dipolar lattice gas, Phys. Rev. Lett. **111**, 185305 (2013).

[9] S. Geier, N. Thaicharoen, C. Hainaut, T. Franz, A. Salzinger, A. Tebben, D. Grimshandl, G. Zürn, and M. Weidemüller, Floquet Hamiltonian engineering of an isolated many-body spin system, Science **374**, 1149 (2021).

[10] P. Scholl, H. J. Williams, G. Bornet, F. Wallner, D. Barredo, L. Henriet, A. Signoles, C. Hainaut, T. Franz, S. Geier, A. Tebben, A. Salzinger, G. Zürn, T. Lahaye, M. Weidemüller, and A. Browaeys, Microwave engineering of programmable XXZ Hamiltonians in arrays of Rydberg atoms, PRX Quantum **3**, 020303 (2022).

[11] L. Christakis, J. S. Rosenberg, R. Raj, S. Chi, A. Morningstar, D. A. Huse, Z. Z. Yan, and W. S. Bakr, Probing site-resolved correlations in a spin system of ultracold molecules, Nature **614**, 64 (2023).

[12] C. Miller, A. N. Carroll, J. Lin, H. Hirzler, H. Gao, H. Zhou, M. D. Lukin, and J. Ye, Two-axis twisting using floquet-engineered XXZ spin models with polar molecules, Nature **633**, 332 (2024).

[13] T. L. Nguyen, J. M. Raimond, C. Sayrin, R. Cortiñas, T. Cantat-Moltrecht, F. Assemat, I. Dotsenko, S. Gleyzes, S. Haroche, G. Roux, T. Jolicoeur, and M. Brune, Towards quantum simulation with circular Rydberg atoms, Phys. Rev. X **8**, 011032 (2018).

[14] D. Barredo, S. de Léséleuc, V. Lienhard, T. Lahaye, and A. Browaeys, An atom-by-atom assembler of defect-free arbitrary two-dimensional atomic arrays, Science **354**, 1021 (2016).

[15] C. Sayrin, Non-destructive optical read-out and local manipulation of circular Rydberg atoms (2025), APS Global Physics Summit (Anaheim, CA), `https://summit.aps.org/events/MAR-G14/5`.

[16] G. D. Mahan, *Many-particle physics*, 3rd ed. (Kluwer, New York, 2000).

[17] R. Samajdar, W. W. Ho, H. Pichler, M. D. Lukin, and S. Sachdev, Quantum phases of Rydberg atoms on a Kagome lattice, Proc. Natl. Acad. Sci. USA **118**, e2015785118 (2021).

[18] D. J. Papoular, See supplemental material at [url will be inserted by publisher] for further theoretical details and computational methods. (2025).

[19] A. Messiah, *Quantum Mechanics, volume II* (North Holland, Amsterdam, 1962).

[20] W. F. Brinkman and R. J. Elliott, Theory of spin-space groups, Proc. R. Soc. (London) A **294**, 343 (1966).

[21] D. B. Litvin and W. Opechowski, Spin groups, Physica **76**, 538 (1974).

[22] L. D. Landau and E. M. Lifshitz, *Quantum Mechanics, non-relativistic theory*, 3rd ed. (Butterworth-Heinemann, Oxford (UK), 1977).

[23] C. J. Bradley and A. P. Cracknell, *The Mathematical Theory of Symmetry in Solids* (Clarendon Press, Oxford, 1972).

[24] A. Messiah, *Quantum Mechanics, volume I* (North Holland, Amsterdam, 1961).

[25] J. H. Eberly, N. B. Narozhny, and J. J. Sanchez-Mondragon, Periodic spontaneous collapse and revival in a simple quantum model, Phys. Rev. Lett. **44**, 1323 (1980).

[26] W. Li, C. Ates, and I. Lesanovsky, Nonadiabatic motional effects and dissipative blockade for Rydberg atoms excited from optical lattices or microtraps, Phys. Rev. Lett. **110**, 213005 (2013).

Measuring the dynamics of an XXZ quantum simulator and controlling collapse through symmetries

SUPPLEMENTAL MATERIAL

D. J. Papoular*

Laboratoire de Physique Théorique et Modélisation, UMR 8089 CNRS & CY Cergy Paris Université, 95302 Cergy–Pontoise, France

(Dated: August 5, 2025)

In this Supplemental Material, we further investigate the assembly of $N = 12$ interacting particles analyzed in the main text. It is organized as follows. In Sec. I, we define the basis $\mathfrak{c}$ comprising 2^N configurations of N particles, and the related bases $\mathfrak{c}^{(M)}$ spanning the subspaces $\mathcal{E}^{(M)}$ characterized by the total spin projection M, with $-N/2 \leq M \leq N/2$. In Sec. II, we discuss the impact of the spin point group symmetry on the eigenstates of the Hamiltonian, considering first the XXZ Hamiltonian $H_{\rm XXZ}$, and then the Heisenberg Hamiltonian $H_{\rm H}$. In particular, we discuss the symmetries of the ground state, and highlight a parameter range in which it is entangled. In Sec. III, we identify a family of factorized N–particle states transforming under the irreducible representation A_{2g} of the spatial symmetry group D_{6h}. The initial states $|\xi\rangle$ and $|\chi\rangle$ considered in the main text belong to this family of experimentally accessible states. In Sec. IV, we discuss the return probabilities for the initial states $|\xi\rangle$ and $|\chi\rangle$, as a function of the ratio J_z/J and the time t. Finally, in Sec. V, we present a full analytical description for the protocol ($\mathcal{P}$) of the main text, involving both time evolution and measurement, in the specific case of an initial state $|\psi_0\rangle$ with the well–defined total spin projection $M = 5$.

Brief summary of the essential notation — The particle i, which has two accessible quantum states $|\uparrow_i^z\rangle$ and $|\downarrow_i^z\rangle$, is confined at the position $\boldsymbol{r}_i$, the N traps being arranged in the (x, y) plane as in Fig. 1 in the main text. The N–particle Hamiltonian, accounting for pairwise interactions decaying like $1/|\boldsymbol{r}_i - \boldsymbol{r}_j|^\alpha$, is given by Eq. 1 in the main text, and reads:

$$H = \frac{1}{2}\sum_{i\neq j}\left(\frac{a}{r_{ij}}\right)^\alpha \left[J(\sigma_i^x\sigma_j^x + \sigma_i^y\sigma_j^y) + J_z\,\sigma_i^z\sigma_j^z\right] . \quad \text{(S1)}$$

where $a = r_{08}$ is the nearest–neighbor distance. The Pauli operators $\boldsymbol{\sigma}_i = (\sigma_i^x, \sigma_i^y, \sigma_i^z)$ represent the qubit at $\boldsymbol{r}_i$, and J, J_z are constant energies. The Hamiltonian $H = H_{\rm H}$ or $H_{\rm XXZ}$ depending on whether $J = J_z$ or $J \neq J_z$.

I. ORDERING OF THE N–PARTICLE CONFIGURATIONS IN THE BASIS $\mathfrak{c}$

We have obtained all of our numerical results (most importantly, Figs. 2 and 3 of the main text) using the basis $\mathfrak{c} = (|c_f\rangle)_{0\leq f\leq 2^N-1}$ containing 2^N configurations of N particles. A given configuration $|c_f\rangle = |\boldsymbol{r}_0, \mu_0; \ldots; \boldsymbol{r}_{N-1}, \mu_{N-1}\rangle = |(\boldsymbol{r}_i, \mu_i)_{0\leq i\leq N-1}\rangle$ is defined by specifying the single–particle internal states $|\mu_i\rangle = |\uparrow_i^z\rangle$ or $|\downarrow_i^z\rangle$ for the particles trapped in each of the sites located at the positions $\boldsymbol{r}_i$, which appear in the ket in order of increasing i.

We first order the single–particle states by ascribing the indices 0 to $|\uparrow^z\rangle$ and 1 to $|\downarrow^z\rangle$. Then, to the N–particle configuration $|(\boldsymbol{r}_i, \mu_i)_{0\leq i\leq N-1}\rangle$ with $\mu_i = \pm 1/2$ as in the main text, we ascribe the index $f = \sum_{i=0}^{N-1}(1/2 - \mu_i)\,2^i$. Hence,

$$\begin{aligned}
|c_0\rangle &= |\uparrow_0, \uparrow_1, \uparrow_2, \uparrow_3, \uparrow_4, \uparrow_5,\ \uparrow_6, \uparrow_7, \uparrow_8, \uparrow_9, \uparrow_{10}, \uparrow_{11}\rangle\ ,\\
|c_1\rangle &= |\downarrow_0, \uparrow_1, \uparrow_2, \uparrow_3, \uparrow_4, \uparrow_5,\ \uparrow_6, \uparrow_7, \uparrow_8, \uparrow_9, \uparrow_{10}, \uparrow_{11}\rangle\ ,\\
&\ \ \vdots\\
|c_{4094}\rangle &= |\uparrow_0, \downarrow_1, \downarrow_2, \downarrow_3, \downarrow_4, \downarrow_5,\ \downarrow_6, \downarrow_7, \downarrow_8, \downarrow_9, \downarrow_{10}, \downarrow_{11}\rangle\ ,\\
|c_{4095}\rangle &= |\downarrow_0, \downarrow_1, \downarrow_2, \downarrow_3, \downarrow_4, \downarrow_5,\ \downarrow_6, \downarrow_7, \downarrow_8, \downarrow_9, \downarrow_{10}, \downarrow_{11}\rangle\ .
\end{aligned} \quad \text{(S2)}$$

In Eq. (S2), the positions $\boldsymbol{r}_0, \ldots, \boldsymbol{r}_{N-1}$ implicitly appear in this order in each of the kets.

The configuration $|c_f\rangle = |(\boldsymbol{r}_i, \mu_i)_{0\leq i\leq N-1}\rangle$ has the well–defined total spin projection $\hbar M$, with $M = \sum_{i=0}^{N-1}\mu_i$. Hence, the full basis $\mathfrak{c}$ may be reorganized into $(N+1)$ bases $\mathfrak{c}^{(M)}$ for the subspaces $\mathcal{E}^{(M)}$, with $-N/2 \leq M \leq N/2$. Within each $\mathfrak{c}^{(M)}$, the configurations are labeled from 0 to $d^{(M)} = \dim\mathcal{E}^{(M)}$ in the same order as in $\mathfrak{c}$. For example, the $d^{(0)} = 924$ configurations with $M = 0$ are labeled as follows:

$$\begin{aligned}
|c_0^{(0)}\rangle &= |\downarrow_0, \downarrow_1, \downarrow_2, \downarrow_3, \downarrow_4, \downarrow_5,\ \uparrow_6, \uparrow_7, \uparrow_8, \uparrow_9, \uparrow_{10}, \uparrow_{11}\rangle\ ,\\
|c_1^{(0)}\rangle &= |\downarrow_0, \downarrow_1, \downarrow_2, \downarrow_3, \downarrow_4, \uparrow_5,\ \downarrow_6, \uparrow_7, \uparrow_8, \uparrow_9, \uparrow_{10}, \uparrow_{11}\rangle\ ,\\
&\ \ \vdots\\
|c_{922}^{(0)}\rangle &= |\uparrow_0, \uparrow_1, \uparrow_2, \uparrow_3, \uparrow_4, \downarrow_5,\ \uparrow_6, \downarrow_7, \downarrow_8, \downarrow_9, \downarrow_{10}, \downarrow_{11}\rangle\ ,\\
|c_{923}^{(0)}\rangle &= |\uparrow_0, \uparrow_1, \uparrow_2, \uparrow_3, \uparrow_4, \uparrow_5,\ \downarrow_6, \downarrow_7, \downarrow_8, \downarrow_9, \downarrow_{10}, \downarrow_{11}\rangle\ ,
\end{aligned} \quad \text{(S3)}$$

where the positions $\boldsymbol{r}_0, \ldots, \boldsymbol{r}_{N-1}$ are implicit as in Eq. (S2). This is the ordering used in Figs. 2 and 3 of the main text.

II. IMPACT OF THE SPIN POINT GROUP SYMMETRY ON THE EIGENSTATES OF H

As discussed in the main text, any spatial symmetry operation (i.e. an element of $G^{\rm spatial}$) may be represented as a permutation ϕ of the N positions $(\boldsymbol{r}_i)$. Under this operation, the N–particle configurations in $\mathfrak{c}$ transform as:

$$|(\boldsymbol{r}_{\phi(i)}, \mu_i)_{0\leq i\leq N-1}\rangle = (-)^\phi\,|(\boldsymbol{r}_i, \mu_{\phi^{-1}(i)})_{0\leq i\leq N-1}\rangle\ , \quad \text{(S4)}$$

* Electronic address: david.papoular@cyu.fr

D_{6h}	E	$2C_6$	$2C_3$	C_2	$3C_2'$	$3C_2''$	I	$2S_3$	$2S_6$	σ_h	$3\sigma_d$	$3\sigma_v$
A_{1g}	1	1	1	1	1	1	1	1	1	1	1	1
A_{2g}	1	1	1	1	-1	-1	1	1	1	1	-1	-1
B_{1g}	1	-1	1	-1	1	-1	1	-1	1	-1	1	-1
B_{2g}	1	-1	1	-1	-1	1	1	-1	1	-1	-1	1
E_{1g}	2	1	-1	-2	0	0	2	1	-1	-2	0	0
E_{2g}	2	-1	-1	2	0	0	2	-1	-1	2	0	0
A_{1u}	1	1	1	1	1	1	-1	-1	-1	-1	-1	-1
A_{2u}	1	1	1	1	-1	-1	-1	-1	-1	-1	1	1
B_{1u}	1	-1	1	-1	1	-1	-1	1	-1	1	-1	1
B_{2u}	1	-1	1	-1	-1	1	-1	1	-1	1	1	-1
E_{1u}	2	1	-1	-2	0	0	-2	-1	1	2	0	0
E_{2u}	2	-1	-1	2	0	0	-2	1	1	-2	0	0

TABLE S1. Character table for the point group D_{6h} (see e.g. Ref. [S1, Appendix II.A]). Each column corresponds to a conjugacy class, and each row to an irreducible representation. Those inapplicable to the considered system are shown in gray.

with $(-)^\phi$ being the parity of ϕ and $|\mu_i\rangle$ the state of the particle originally at position $\boldsymbol{r}_i$.

	A_{1g}	A_{2g}	E_{2g}	B_{1u}	B_{2u}	E_{1u}	Total
$M=\pm6$	0	1	0	0	0	0	$\binom{12}{0}=1$
$M=\pm5$	0	2	2×2	1	1	2×2	$\binom{12}{1}=12$
$M=\pm4$	3	9	2×12	5	5	2×10	$\binom{12}{2}=66$
$M=\pm3$	14	24	2×36	19	19	2×36	$\binom{12}{3}=220$
$M=\pm2$	35	50	2×85	40	40	2×80	$\binom{12}{4}=495$
$M=\pm1$	56	76	2×132	66	66	2×132	$\binom{12}{5}=792$
$M=0$	70	90	2×156	76	76	2×150	$\binom{12}{6}=924$
Total	286	414	2×690	338	338	2×670	$2^{12}=4096$

TABLE S2. Analytical prediction for the number of eigenstates of H simultaneously belonging to *(i)* the irreducible representation ρ of D_{6h} and *(ii)* the eigenspace of S_z with eigenvalue $\hbar M$. The integer M satisfies $-N/2 \leq M \leq N/2$. For any ρ and $M \neq 0$, the symmetry classes (ρ, M) and $(\rho, -M)$ contain the same number of states.

A. Relevant representations of D_{6h}

Regardless of whether $J \neq J_z$ or $J = J_z$, the point group G^{spatial}, acting on the site positions while leaving the spins unaffected, is D_{6h} [S2, §93]. This group has 12 inequivalent irreducible representations [S1, Appendix II.A.6], and Table S1 gives its character table. Only some representations are relevant to the description of the considered system. Indeed, let us consider the mirror σ_h, which leaves invariant each point in the horizontal plane within which all atoms lie ((x, y) plane of Fig. 1 in the main text). By definition of the symmetry elements in G^{spatial}, it also leaves the spins invariant. Hence, it should act as the identity. Therefore, its character in any irreducible representation applicable to the considered system should be the dimension of this representation. The character table of D_{6h} (see Table S1) shows that six representations satisfy this criterion: A_{1g}, A_{2g}, B_{1u}, B_{2u} (which are unidimensional) and E_{2g}, E_{1u} (which are bidimensional).

Dimension	1	2	4
# Eigenspaces	312	838	527

TABLE S3. Degeneracies of the XXZ model (geometry of Fig. 1 in the main text). The bottom line gives the number of eigenspaces whose dimensions appear on the first line.

B. Dimensions of the blocks representing the various symmetry classes

The group D_{6h} acts on the full Hilbert space $\mathcal{H}$ as a reducible representation. We calculate the array of the characters of the 24 group elements for this representation. Its scalar product with the corresponding arrays for each of the irreducible representations ρ of D_{6h} yields the total number of eigenstates of the Hamiltonian H (Eq. 1 of the main text) transforming under ρ [S2, §94], given in the last line of Table S2. Similarly, for any integer M such that $-N/2 \leq M \leq N/2$, the subspace $\mathcal{E}_M$ of $\mathcal{H}$ characterized by the total spin projection $S_z = M$ is stable under the action of D_{6h}, and we obtain the number of eigenstates of the Hamiltonian in this subspace transforming under each ρ in the same way (remainder of Table S2). For the XXZ Hamiltonian, this is the dimension of the block labeled (ρ, M) in the main text.

The symmetry group G_{XXZ} yields degeneracies through two different mechanisms. Firstly, the irreducible representations E_{2g} and E_{1u} of D_{6h} are bidimensional. Secondly, G^{spin} contains the rotation $C_2^{\boldsymbol{e}_x,\text{spin}}$ about the axis $\boldsymbol{e}_x$ through the angle π, simultaneously acting on the spins of all $N = 12$ particles.

It transforms the quantum state of each spin–1/2 according to $|\uparrow\rangle \to -i\,|\downarrow\rangle$ and $|\downarrow\rangle \to -i\,|\uparrow\rangle$. Using $(-i)^{12} = 1$, we find that $C_2^{e_x,\mathrm{spin}}$ acts as the spin–flip operator. Therefore, any eigenstate $|\Psi\rangle$ of H with total spin projection $M \neq 0$ is degenerate with $C_2^{e_x}\,|\Psi\rangle$, which is an eigenstate of H with total spin projection $-M$. Combining these two properties, the eigenspaces of H have dimension 1, 2, and 4: the corresponding numbers of eigenspaces are given in Table S3.

C. Specific case of the Heisenberg model

We now consider the specific case of $J_z = J$. This has two consequences. First, the total spin $\boldsymbol{S}^2$ is conserved, and the blocks are now labeled by (ρ, S, M), where the integer S satisfies $|M| \leq S \leq N/2$ and sets the spin modulus $\boldsymbol{S}^2 = \hbar^2 S(S+1)$. Second, an additional mechanism yielding degeneracies is active. The operator $S^+ = S_x + iS_y$ commutes with H, so that the spectrum of H is comprised of multiplets of $(2S+1)$ degenerate states with total spin S. The number of spin–S multiplets in each representation ρ, obtained from Table S2 as the difference between the numbers of eigenstates with $M = S$ and $M = (S+1)$ [S2, §63, Problem 1], is given in Table S4. The degeneracies resulting from the three mechanisms at play are summarized in Table S5.

	A_{1g}	A_{2g}	E_{2g}	B_{1u}	B_{2u}	E_{1u}	Total
$S=6$	0	1	0	0	0	0	$\binom{12}{0} = 1$
$S=5$	0	1	2×2	1	1	2×2	$\binom{12}{1} - \binom{12}{0} = 11$
$S=4$	3	7	2×10	4	4	2×8	$\binom{12}{2} - \binom{12}{1} = 54$
$S=3$	11	15	2×24	14	14	2×26	$\binom{12}{3} - \binom{12}{2} = 154$
$S=2$	21	26	2×49	21	21	2×44	$\binom{12}{4} - \binom{12}{3} = 275$
$S=1$	21	26	2×47	26	26	2×52	$\binom{12}{5} - \binom{12}{4} = 297$
$S=0$	14	14	2×24	10	10	2×18	$\binom{12}{6} - \binom{12}{5} = 132$

TABLE S4. Heisenberg model: analytical prediction for the number of multiplets with total spin S in each irreducible representation ρ of D_{6h}. The integer S satisfies $0 \leq S \leq N/2$. Each multiplet is comprised of $(2S+1)$ degenerate eigenstates.

Dimension	1	2	3	5	6	7	9	10	11	13	14	18	22
# Eigenspaces	48	42	99	89	99	54	18	93	3	1	50	18	4

TABLE S5. Degeneracies of the Heisenberg model (geometry of Fig. 1 in the main text). The bottom line gives the number of eigenspaces whose dimensions appear on the first line.

Numerical calculations — For a given value of J_z/J, we express H in the basis $\mathfrak{c}$ comprised of the 2^N states $|r_0, \mu_0; \ldots; r_{N-1}, \mu_{N-1}\rangle$, with $|\mu_i\rangle = |\uparrow_i^z\rangle$ or $|\downarrow_i^z\rangle$ for each particle i, and numerically diagonalize the resulting real symmetric 4096×4096 matrix. We have checked numerically, for interactions decaying like $1/d^\alpha$ with d being the interparticle distance, with $\alpha = 3$ and 6, and for $-3 \leq J_z/J \leq 3$, that the degeneracies of the energy spectrum of H are those predicted in Tables S3 and S5.

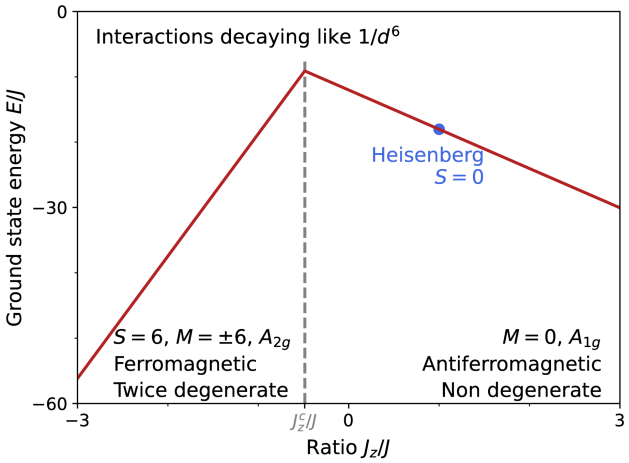

FIG. S1. Ground state energy E/J as a function of J_z/J, calculated for interactions decaying like $1/d^6$. The change in the symmetry of the ground state wavefunction occurs for $J_z/J \approx -0.485$ (dashed vertical line).

The time–dependent measurement probabilities, illustrated on Figs. 2 and 3 of the main text and calculated from Eq. 3 there, are obtained by projecting the initial state $|\psi_0\rangle$ onto the eigenstates of H, and accounting for the time–dependent phase resulting from their evolution in time.

We have performed all these calculations using NumPy [S3]. Figures 2 and 3 of the main text were obtained within a few minutes on a recent desktop computer (128 GB of RAM; Intel Xeon CPU with the speed 3.50 GHz and 24 threads).

D. Ground state energy, symmetry, and entanglement

In this subsection, we focus on the ground state of H. Figure S1 represents the dependence of the ground state energy E_{GS}/J on the ratio J_z/J. It behaves linearly for $J_z < J_z^c$, where $J_z^c/J \approx -0.486$, and nearly linearly for $J_z > J_z^c$. The slope dE_{GS}/dJ_z is positive in the first region and negative in the second one, signaling a change in the symmetry of the ground–state wavefunction.

For $J_z < J_z^c$, the ground state is exactly ferromagnetic and twice degenerate. The ground–state eigenspace is spanned by the N–particle wavefunctions $|\uparrow_0 \ldots \uparrow_{N-1}\rangle$ and $|\downarrow_0 \ldots \downarrow_{N-1}\rangle$. The total spin projection satisfies $|M| = N/2$, hence, the total spin modulus is also well defined, $S = N/2$. All states in the ground–state eigenspace transform under G^{spatial} according to the irreducible representation A_{2g} (see Table S1). The minus sign entering the character of some group elements in this representation stems from Eq. (S4).

For $J_z > J_z^c$, we numerically find that the ground state is antiferromagnetic and belongs to the symmetry class $(A_{1g}, M = 0)$. Hence, it is non–degenerate. In the specific Heisenberg case $J_z = J$, the ground–state wavefunction $|\Psi_{\mathrm{GS}}^{\mathrm{H}}\rangle$ belongs to

the block labeled (A_{1g}, $S = 0$, $M = 0$) which, according to Table S4, has dimension 14. For $J_z \neq J$, the ground–state wavefunction $|\Psi_{\rm GS}\rangle$ no longer has a well–defined value of S, and acquires small components along $S = 2$ and $S = 4$. However, it remains very close to $|\Psi^{\rm H}_{\rm GS}\rangle$: for $\alpha = 6$ and $J^c_z < J_z < 3$, the squared overlap $|\langle\Psi^H_{GS}|\Psi_{GS}\rangle|^2 > 0.995$.

Finally, we discuss the presence or not of entanglement in the ground state. In the ferromagnetic case ($J_z < J^c_z$), the system may be prepared in a ground–state wavefunction with well–defined spin projection $M = +6$ or -6. Then, the ground–state wavefunction is a tensor product of single–particle wavefunctions, so that it is not entangled. The situation is different in the antiferromagnetic case ($J_z > J^c_z$). For a given value of J_z/J, we numerically calculate the Schmidt number [S4, §2.5] of the ground state with respect to each of the bipartite partitions of the N qubits. For all considered values $J^c_z/J < J_z/J < 3$, this number is ≥ 2 for all partitions, so that the ground state is entangled.

Numerical calculation of the Schmidt number — For any integer p such that $0 \leq p \leq 2^N - 1$, with the binary decomposition $\sum_{i=0}^{N-1} p_i\, 2^i$, the bipartite partition with index p is defined as follows: the qubit on site i is of type A if $p_i = 0$ and of type B if $p_i = 1$. This generates all 2^N bipartite partitions of the N qubits. However, only $2^{N-1} - 1$ partitions need be tested, because of the following two reasons. *(i)* The partitions with extremal indices $p = 0$ and 2^{N-1} correspond to all qubits being of the same type A or B and, hence, do not probe for entanglement. *(ii)* Simultaneously exchanging all qubits of type A with all qubits of type B leads to the same Schmidt rank.

For a given bipartite partition with N_a qubits of type A and N_b qubits of type B, such that $N_a + N_b = N$, we reshape the vector with 2^N components representing the ground state of the system into a matrix with 2^{N_a} lines and 2^{N_b} columns, labeled by the basis states for the particles of type A and B, respectively. This is achieved using bit rearrangement techniques presented in [S5, chap. 7]. The Schmidt number is the number of non–vanishing singular values of this matrix [S4, Sec. 2.5], which we calculate using Numpy [S3].

III. A FAMILY OF FACTORIZED N–PARTICLE STATES TRANSFORMING ACCORDING TO A_{2g}

In this section, we identify a family of N–particle states $|\zeta\rangle$ which are products of single–particle states and which tranform under spatial symmetry operations according to the irreducible representation A_{2g}. Their definition exploits the double–ring structure of Fig. 1 in the main text, detailed in Fig. S2 of the present document.

A. Definition of the states $|\zeta\rangle$

We choose two single–particle internal states $|\mu_{\rm outer}\rangle$ and $|\mu_{\rm inner}\rangle$, each of which is an arbitrary superposition of $|\uparrow^z\rangle$ and $|\downarrow^z\rangle$. We define the N–particle state $|\zeta\rangle$ such that all particles on the outer ring (red sites in Fig. S2) are in the state $|\mu_{\rm outer}\rangle$

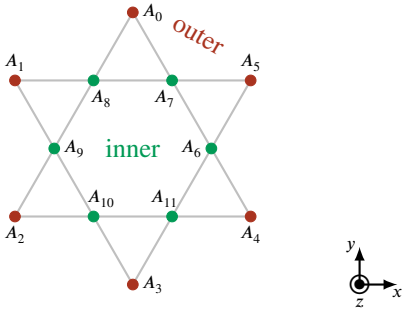

FIG. S2. The considered system: twelve interacting particles trapped in the (x, y) plane in a regular double–ring geometry. The six sites of the outer ring appear in red, and those of the inner ring in green.

and all those on in the inner ring (green sites in Fig. S2) are in the state $|\mu_{\rm inner}\rangle$:

$$|\zeta\rangle \;=\; |(\boldsymbol{r}_j, \mu_{\rm outer})_{0\leq j\leq N/2-1}\,;\,(\boldsymbol{r}_k, \mu_{\rm inner})_{N/2\leq k\leq N-1}\rangle\;. \tag{S5}$$

The states $|\xi\rangle$ and $|\chi\rangle$ considered in the main text belong to this family. Indeed, the choice $|\mu_{\rm outer}\rangle = |\mu_{\rm inner}\rangle = |\uparrow^x\rangle$ yields $|\xi\rangle$, while $|\mu_{\rm outer}\rangle = |\uparrow^x\rangle$, $|\mu_{\rm inner}\rangle = |\uparrow^z\rangle$ yields $|\chi\rangle$.

B. Behavior under spatial symmetry operations

We act on the state $|\zeta\rangle$ with a spatial symmetry operation g represented by the permutation ϕ. This operation leaves both the outer ring and the inner ring globally invariant, hence, Eq. (S4) yields $g\,|\xi\rangle = (-)^\phi\,|\xi\rangle$. Therefore, all elements in a given conjugacy class of D_{6h} act in the same way. We examine these twelve classes in turn.

The identity E satisfies $E\,|\zeta\rangle = +\,|\zeta\rangle$.

The rotation shifting the atoms on each ring counterclockwise by one site, which belongs to class C_6, is represented by the permutation

$$\begin{pmatrix}0&1&2&3&4&5\\1&2&3&4&5&0\end{pmatrix}\begin{pmatrix}6&7&8&9&10&11\\7&8&9&10&11&6\end{pmatrix}\,, \tag{S6}$$

whose parity is $[(-1)^5]^2 = +1$. Hence, $C_6\,|\zeta\rangle = |\zeta\rangle$. This also entails $C_3\,|\zeta\rangle = |\zeta\rangle$ and $C_2\,|\zeta\rangle = |\zeta\rangle$.

The rotation about the axis (Ox), which belongs to class C_2', is represented by the permutation

$$\begin{pmatrix}0&1&2&3&4&5\\3&2&1&0&5&4\end{pmatrix}\begin{pmatrix}6&7&8&9&10&11\\6&11&10&9&8&7\end{pmatrix}\,, \tag{S7}$$

whose parity is $(-1)^5 = -1$. Hence, $C_2'\,|\zeta\rangle = -\,|\zeta\rangle$. Similarly, $C_2''\,|\zeta\rangle = -\,|\zeta\rangle$.

Spatial inversion I is represented by the permutation

$$\begin{pmatrix}0&1&2&3&4&5\\3&4&5&0&1&2\end{pmatrix}\begin{pmatrix}6&7&8&9&10&11\\9&10&11&6&7&8\end{pmatrix}\,, \tag{S8}$$

whose parity is $(-1)^6 = +1$. Hence, $I\,|\zeta\rangle = +\,|\zeta\rangle$.

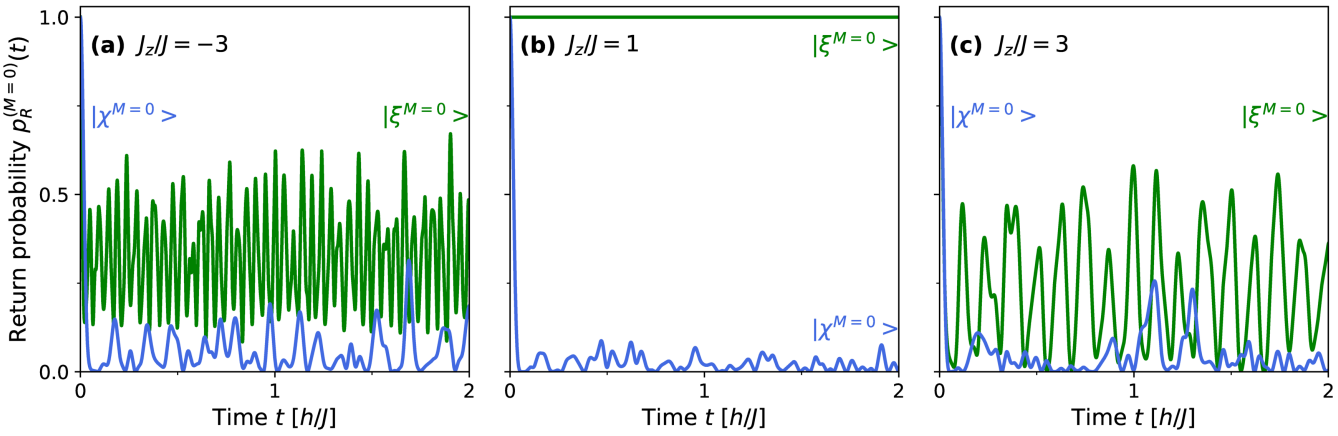

FIG. S3. Return probability $p_R^{(M=0)}(t)$ for the initial states $|\psi_0\rangle = |\xi^{(M=0)}\rangle$ (green) and $|\chi^{(M=0)}\rangle$ (blue), evolving under the Hamiltonian of Eq. 1 in the main text with $\alpha = 6$ and $J_z/J =$ (a) -3, (b) 0, and (c) $+3$, normalized such that $p_R^{(M=0)}(0) = 1$.

The classes S_3 and S_6, comprised of rotary–reflections, and the reflection σ_h through the horizontal plane (Oxy), satisfy the relations $S_3 = IC_6$, $S_6 = IC_3$, and $\sigma_h = IC_2$. These yield $S_3|\zeta\rangle = S_6|\zeta\rangle = \sigma_h|\zeta\rangle$. Similarly, the classes σ_d and σ_h, comprised of reflections through planes containing the axis (Oz), satisfy the relations $\sigma_d = IC_2'$, and $\sigma_v = IC_2''$. These yield $\sigma_d|\zeta\rangle = \sigma_v|\zeta\rangle = -|\zeta\rangle$.

Confronting these twelve transformation laws to the character table of D_{6h} (Table S1), we conclude that $|\zeta\rangle$ transforms according to the representation A_{2g}.

IV. RETURN PROBABILITY

We assume that the system is prepared in the initial state $|\psi_0\rangle$, and let it evolve under the Hamiltonian of Eq. 1 in the main text. Then, the probability that the quantum state at time t return to $|\psi_0\rangle$ is $p_R(t) = |\langle\psi_0|\psi(t)\rangle|^2$, where:

$$\langle\psi_0|\psi(t)\rangle = \sum_\nu \exp(-iE_\nu t/\hbar)\,|\langle\Psi_\nu|\psi_0\rangle|^2\,. \tag{S9}$$

In Eq. (S9), the $(|\Psi_\nu\rangle)_{0\le\nu\le N-1}$ are the eigenstates of H, with energies (E_ν), just like in Eq. 3 of the main text. We illustrate these return probabilities in Fig. S3 for the components $|\xi^{(M=0)}\rangle$ and $|\chi^{(M=0)}\rangle$ of the states $|\xi\rangle$ and $|\chi\rangle$ defined in Sec. III A above, for $\alpha = 6$ and three different values of J_z/J. In the case of $|\xi^{(M=0)}\rangle$, the return probability $p_R^{|\xi\rangle}$ is constant if $J_z = J$, in accordance with the fact that the initial state is an eigenstate of $H_{\rm H}$. However, if $J_z/J \neq 1$, $p_R^{|\xi\rangle}(t)$ oscillates aperiodically as a function of time, with comparable amplitudes for $J_z/J = 3$ and -3. In the case of $|\chi^{(M=0)}\rangle$, the return probability $p_R^{|\chi\rangle}(t)$ collapses to very small values for $t \lesssim 0.05h/J$, and subsequently oscillates aperiodically. The amplitude of this second regime is the smallest for $J_z/J = 1$, in which case $p_R^{|\chi\rangle}(t) \lesssim 0.1$. This justifies the choice of $J_z/J = 1$ for Fig. 3 in the main text.

V. ANALYTICAL SOLUTION WITHIN $\mathcal{E}^{(M=5)}$

In this section, we assume as in the main text that the initial state $|\psi_0\rangle$ transforms according to the irreducible representation A_{2g}, and focus on the subspace $\mathcal{E}^{(M=5)}$ comprising all configurations with total spin projection $M = 5$. In this context, we present a fully analytical description of the protocol $\mathcal{P}$ analyzed in the main text. This solution exists because the block $(A_{2g}, M = 5)$ has dimension 2 (see Table S2), so that the Hamiltonian governing the evolution within this block is a 2×2 matrix. Our analytical results are in perfect agreement with Figs. 2a and 3a of the main text, obtained numerically.

A. Configurations in $\mathcal{E}^{(M=5)}$

The subspace $\mathcal{E}^{(M=5)}$ has dimension $d^{(5)} = \binom{12}{1}$, which is the number of ways to flip a single spin among 12. It is spanned by the basis $\mathfrak{c}^{(M=5)}$ comprising the following 12 configurations $|c_f^{(5)}\rangle$, with $0 \le f \le 11$:

$$|c_f^{(5)}\rangle = |\boldsymbol{r}_0, \mu_0; \boldsymbol{r}_1, \mu_1; \ldots; \boldsymbol{r}_{11}, \mu_{11}\rangle\,, \tag{S10}$$

where $|\mu_i\rangle = |\downarrow_i^z\rangle$ for $i = f$ and $|\uparrow_i^z\rangle$ for $i \neq f$. This is the ordering used in Figs. 2a and 3a of the main text.

The block $(A_{2g}, M = 5)$, which is a symmetry class of $H_{\rm XXZ}$, has dimension $d^{(5)}_{A_{2g}} = 2$ (see Table S2). It is spanned by the basis comprising the N–particle kets $|e^{(5)}_{\rm outer}\rangle$ and $|e^{(5)}_{\rm inner}\rangle$:

$$|e^{(5)}_{\rm outer}\rangle = \frac{1}{\sqrt{6}}\sum_{f=0}^{5}|c_f^{(5)}\rangle \text{ and } |e^{(5)}_{\rm inner}\rangle = \frac{1}{\sqrt{6}}\sum_{f=6}^{11}|c_f^{(5)}\rangle\,. \tag{S11}$$

In Eq. (S11), $|e^{(5)}_{\rm outer}\rangle$ is the symmetric sum of all six configurations comprising a single particle in the state $|\downarrow^z\rangle$ positioned on the outer ring (i.e. on one of the red sites of Fig. S2), and

$|e^{(5)}_{\text{inner}}\rangle$ is the equivalent state for the inner ring (green sites of Fig. S2). Neither $|e^{(5)}_{\text{outer}}\rangle$ nor $|e^{(5)}_{\text{inner}}\rangle$ belongs to the basis $\mathfrak{c}^{(5)}$.

We follow the protocol ($\mathcal{P}$) of the main text. We start from the initial state $|\psi_0\rangle$, which in the present section is chosen in $\mathcal{E}^{(M=5)}$. We let the system evolve under the Hamiltonian H which may be either H_{H} or H_{XXZ}: the N–particle state $|\psi(t)\rangle$ remains within $\mathcal{E}^{(M=5)}$ at all times. Finally, we measure it at time t in the basis $\mathfrak{c}^{(M=5)}$.

The probability $p^{(5)}_f(t)$ of finding the configuration $|c^{(5)}_f\rangle$ is given by Eq. 3 of the main text. The configurations enter this equation only through the overlaps $\langle c^{(5)}_f|e^{(5)}_{\text{outer}}\rangle$ and $\langle c^{(5)}_f|e^{(5)}_{\text{inner}}\rangle$. Hence, at any given time t, the six configurations $|c^{(5)}_f\rangle$ for $0 \leq f \leq 5$ are equiprobable, their shared probability being $p^{(5)}_{\text{inner}}(t) = |\langle c^{(5)}_f|\psi(t)\rangle|^2$. Similarly, the $|c^{(5)}_f\rangle$'s for $6 \leq f \leq 11$ are equiprobable, with probability $p^{(5)}_{\text{outer}}(t)$.

B. Heisenberg Hamiltonian H_{H}

For the Heisenberg Hamiltonian, the block $(A_{2g}, M = 5)$ comprises the two symmetry classes $(A_{2g}, S = 6, M = 5)$ and $(A_{2g}, S = 5, M = 5)$, each of which is unidimensional (see Table S4). The basis vector $|A_{2g}, S = 6, M = 5\rangle$ is obtained by applying the spin lowering operator $S^- = \sum_{i=0}^{N-1} s_i^-$ to the fully polarized state $|(\boldsymbol{r}_i, \uparrow^z_i)_{0\leq i\leq N-1}\rangle$ with all N spins pointing along $|\uparrow^z\rangle$:

$$|A_{2g}, S = 6, M = 5\rangle = (|e^{(5)}_{\text{outer}}\rangle + |e^{(5)}_{\text{inner}}\rangle)/\sqrt{2}\,. \quad \text{(S12)}$$

As for $(A_{2g}, S = 5, M = 5)$, we may choose as a basis vector any linear combination of $|e^{(5)}_{\text{outer}}\rangle$ and $|e^{(5)}_{\text{inner}}\rangle$ which is orthogonal to $|S = 6, M = 5\rangle$, say:

$$|A_{2g}, S = 5, M = 5\rangle = (-|e^{(5)}_{\text{outer}}\rangle + |e^{(5)}_{\text{inner}}\rangle)/\sqrt{2}\,. \quad \text{(S13)}$$

All N–particle states with the quantum numbers $S = 6$, $M = 5$ are proportional to $|A_{2g}, S = 6, M = 5\rangle$, whereas there are 11 orthogonal states with the quantum numbers $S = 5$, $M = 5$, transforming under various representations (see Table S4).

The blocks $(A_{2g}, S, M = 5)$ for $S = 6$ and 5 both have dimension 1, hence, the N–particle states $|S = 6, M = 5\rangle$ and $|A_{2g}, S = 5, M = 5\rangle$ are eigenstates of H_{H} regardless of the value of α. The difference $\Delta E = E_{S=6} - E_{A_{2g},S=5}$ of the two corresponding eigenvalues satisfies:

$$\Delta E/J = 8\,(1 + 2^{-\alpha} + 7^{-\alpha/2})\,. \quad \text{(S14)}$$

We choose $|\psi_0\rangle = |\chi^{(5)}\rangle/\|\chi^{(5)}\| = |e^{(5)}_{\text{outer}}\rangle$ like for Fig. 3a of the main text. Then, Eq. 3 of the main text leads to:

$$\begin{aligned} p^{(5)}_{\text{outer}}(t) &= \frac{1}{6}\cos^2[\Delta E\, t/(2\hbar)]\,, \\ p^{(5)}_{\text{inner}}(t) &= \frac{1}{6}\sin^2[\Delta E\, t/(2\hbar)]\,. \end{aligned} \quad \text{(S15)}$$

For $\alpha = 6$, Eq. (S14) yields the exact result $\Delta E/J = 22359/2744 \approx 8.2$, and the analytical Eq. (S15) perfectly matches the numerical results of Fig. 3a of the main text.

C. XXZ Hamiltonian H_{XXZ}

The $(A_{2g}, M = 5)$ block may be solved analytically even if $J_z \neq J$. Then, the total spin modulus S is not conserved, and the two eigenstates of H_{XXZ} within this block depend on both J/J_z and α. We first consider the specific values $J_z/J = -3$ and $\alpha = 6$, corresponding to Fig. 2a of the main text, then generalize our results to arbitrary values of J_z/J and α.

1. *Results for $J_z/J = -3$ and $\alpha = 6$*

First, we focus on the specific values $J_z/J = -3$ and $\alpha = 6$, as in Fig. 2a of the main text. Expressing the restriction $\widetilde{H}_{\text{XXZ}}$ of H_{XXZ} in the basis $\mathfrak{c}^{(5)}$, we find the exact result:

$$\begin{aligned} \frac{\widetilde{H}_{\text{XXZ}}}{J} &= \begin{pmatrix} -173351219/4000752 & 22359/5488 \\ 22359/5488 & -12105047/444528 \end{pmatrix} \\ &\approx \begin{pmatrix} -43.3 & 4.1 \\ 4.1 & -27.2 \end{pmatrix}. \end{aligned} \quad \text{(S16)}$$

The probabilities $p^{(5)}_{\text{outer}}(t)$ and $p^{(5)}_{\text{inner}}(t)$ obtained from the initial state $|\xi^{(5)}\rangle/\|\xi^{(5)}\| = (|e^{(5)}_{\text{outer}}\rangle + |e^{(5)}_{\text{inner}}\rangle)/\sqrt{2}$ undergo sinusoidal oscillations at the same frequency, set by the difference ΔE_{XXZ} of the two eigenvalues of $\widetilde{H}_{\text{XXZ}}$, exactly given by:

$$\frac{\Delta E_{\text{XXZ}}}{J} = -5\frac{\sqrt{52108288731277}}{2000376} \approx -18.0\,. \quad \text{(S17)}$$

The probabilities $p^{(5)}_{\text{outer}}(t)$ and $p^{(5)}_{\text{inner}}(t)$ obtained from the analytical Eqs. (S16) and (S17) are in perfect agreement with the numerical results of Fig. 2a in the main text.

2. *General analytical description of the $(A_{2g}, M = 5)$ block*

We now turn to the general case, where J_z/J and α may take arbitrary values. Eq. (S16) generalizes to:

$$\frac{\widetilde{H}_{\text{XXZ}}}{J} = \begin{pmatrix} h^{(0)}_{11} & h^{(0)}_{12} \\ h^{(0)}_{21} & h^{(0)}_{22} \end{pmatrix} + \frac{J_z}{J}\begin{pmatrix} h^{(1)}_{11} & 0 \\ 0 & h^{(1)}_{22} \end{pmatrix}, \quad \text{(S18)}$$

where the matrix elements $h^{(0)}_{ij}$ read:

$$\begin{aligned} h^{(0)}_{11} &= 4\times 3^{-\alpha} + 4\times 3^{-\alpha/2} + 2^{1-\alpha}\times 3^{-\alpha/2}\,, \\ h^{(0)}_{12} &= h^{(0)}_{21} = 4\left(1 + 2^{-\alpha} + 7^{-\alpha/2}\right)\,, \\ h^{(0)}_{22} &= 4 + 4\times 3^{-\alpha/2} + 2^{1-\alpha}\,, \end{aligned} \quad \text{(S19)}$$

and the diagonal coefficients $h^{(1)}_{ii}$ are given by:

$$\begin{aligned} h^{(1)}_{11} &= 14 + 11\times 2^{-\alpha} + 2\times 3^{-\alpha} + 8\times 3^{-\alpha/2} \\ &\quad + 2^{-\alpha}\times 3^{-\alpha/2} + 8\times 7^{-\alpha/2}\,, \\ h^{(1)}_{22} &= 10 + 9\times 2^{-\alpha} + 6\times 3^{-\alpha} + 8\times 3^{-\alpha/2} \\ &\quad + 3\times 2^{-\alpha}\times 3^{-\alpha/2} + 8\times 7^{-\alpha/2}\,. \end{aligned} \quad \text{(S20)}$$

Finally, the energy difference of Eq. (S17), which determines the shared frequency at which the probabilities $p^{(5)}_{\text{outer}}(t)$ and $p^{(5)}_{\text{inner}}(t)$ oscillate sinusoidally, becomes:

$$\frac{\Delta E_{\text{XXZ}}}{J} = \sqrt{\kappa^{(0)} + \kappa^{(1)} \frac{J_z}{J}\left(\frac{J_z}{J} - 2\right)}, \tag{S21}$$

where the coefficients $\kappa^{(0)}$ and $\kappa^{(1)}$ read:

$$\begin{aligned}
\kappa^{(0)} &= 80 \\
&\quad + 2^{4-\alpha}(9 + 3^{-3\alpha/2} - 3^{-\alpha} - 3^{-\alpha/2} + 8 \times 7^{-\alpha/2}) \\
&\quad + 4^{1-\alpha}(17 + 3^{-\alpha} - 2 \times 3^{-\alpha/2}) - 32 \times 3^{-\alpha} \\
&\quad + 64 \times 7^{-\alpha} + 128 \times 7^{-\alpha/2} + 16 \times 9^{-\alpha}\,, \\
\kappa^{(1)} &= 4^{1-\alpha} \times 9^{-\alpha}\left(2^{1+\alpha} + 3^{\alpha/2} - 3^{\alpha}(1 + 2^{1+\alpha})\right)^2\,.
\end{aligned} \tag{S22}$$

[S1] F. A. Cotton, *Chemical applications of group theory*, 3rd ed. (Wiley, New York, 1990).
[S2] L. D. Landau and E. M. Lifshitz, *Quantum Mechanics, non-relativistic theory*, 3rd ed. (Butterworth-Heinemann, Oxford (UK), 1977).
[S3] C. R. Harris *et al.*, Array programming with NumPy, Nature **585**, 357 (2020).
[S4] M. A. Nielsen and I. L. Chuang, *Quantum Computation and Quantum Information* (Cambridge University Press, Cambridge (UK), 2000).
[S5] J. H. S. Warren, *Hacker's Delight*, 2nd ed. (Pearson Education (New Jersey), 2013).